Journal of Cerebral Blood Flow and Metabolism
11:10–24 © 1991 Raven Press, Ltd., New York

Model of Kinetic Behavior of Deoxyglucose in Heterogeneous Tissues in Brain: A Reinterpretation of the Significance of Parameters Fitted to Homogeneous Tissue Models

K. Schmidt, *G. Mies, and L. Sokoloff

*Laboratory of Cerebral Metabolism, National Institute of Mental Health, U.S. Department of Health and Human Services, Public Health Service, Bethesda, Maryland, U.S.A.; and *Department of Experimental Neurology, Max Planck Institute for Neurological Research, Cologne, F.R.G.*

Summary: Effects of tissue heterogeneity on regional CMR_{glc} ($rCMR_{glc}$) calculated by use of the deoxyglucose (DG) method at 45 min following the pulse of DG were evaluated in simulation studies. A theoretical model was developed to describe the kinetics of DG uptake and metabolism in heterogeneous brain tissues. Rate constants were fitted to simulation data for mixed tissue and $rCMR_{glc}$ computed on the basis of this tissue heterogeneity model. The results were compared with those obtained by use of the original model of the DG method for homogeneous tissue, both without (3K model) and with (4K model) a term to describe an apparent loss of deoxyglucose-6-phosphate (DG-6-P). As a direct consequence of tissue heterogeneity, the effective rate constant for phosphorylation of DG, k_3^*, declined with time. To compensate for the time-changing k_3^*, estimates of the dephosphorylation rate constant, k_4^*, were artifactually high when the 4K model was used, even though no dephosphorylation of DG-6-P actually occurred. The present study demonstrates that the finding of a significant k_4^*, at least within 45 min following a pulse of DG, may not represent dephosphorylation at all, but rather the consequence of measuring radioactivity in a heterogeneous tissue and applying a model designed for a homogeneous tissue. Furthermore, the high estimates of k_4^* resulted in significant overestimation of $rCMR_{glc}$. When $rCMR_{glc}$ was computed with the conventional single-scan or autoradiographic method at 45 min after a pulse of DG, the 3K and tissue heterogeneity models yielded values that were within 5% of the true weighted average value for the heterogeneous tissue as a whole. We conclude that the effects of tissue heterogeneity alone can give the appearance of product loss, even when none occurs, and that the use of the 4K model with the assumption of product loss in the 45-min experimental period recommended for the DG method may lead to overestimation of the rates of glucose utilization. **Key Words:** Apparent glucose-6-phosphatase activity—k_4^*—Modeling—Rate constant estimation—Rate constants.

Received March 2, 1990; revised May 2, 1990; accepted May 4, 1990.

Address correspondence and reprint requests to K. Schmidt at Laboratory of Cerebral Metabolism, National Institute of Mental Health, Building 36, Room 1A-05, 9000 Rockville Pike, Bethesda, MD 20892, U.S.A.

Portions of this work were presented in preliminary form at the 14th International Symposium on Cerebral Blood Flow and Metabolism (Brain '89), Bologna, Italy, May 28–June 1, 1989 (Schmidt et al., 1989*b*).

Abbreviations used: DG, deoxyglucose; DG-6-P, deoxyglucose-6-phosphate; FDG, fluorodeoxyglucose; $LCMR_{glc}$, local CMR_{glc}; PET, positron emission tomography; $rCMR_{glc}$, regional CMR_{glc}.

The kinetic model of the deoxyglucose (DG) method for the measurement of local CMR_{glc} ($LCMR_{glc}$) specifically applies only to a localized region of tissue that is homogeneous with respect to rates of blood flow, transport of hexoses across the blood–brain barrier, glucose metabolism, DG phosphorylation, and concentrations of DG, glucose, deoxyglucose-6-phosphate (DG-6-P), and glucose-6-phosphate (Sokoloff et al., 1977). The original two-compartment, three–rate constant (3K) model assumes that DG-6-P, once formed, is effectively

trapped in the tissue for the duration of the experimental period. The recommended experimental period of 45 min was, in fact, chosen to be long enough to minimize the influence of the model rate constants on the calculated rate of glucose utilization and yet short enough for loss of product to remain insignificant. The findings that $LCMR_{glc}$ calculated between 30 and 45 min following a pulse of DG remains relatively constant and that the values are consistent with those for global cerebral glucose utilization measured by the Kety-Schmidt technique supported the assumption that DG-6-P and its metabolic products remain essentially trapped in the tissue during that period (Sokoloff et al., 1977). More recently, direct experimental evidence has validated this assumption (Sokoloff, 1982, 1985; Nelson et al., 1987; Mori et al., 1990) and confirmed that it is not necessary to consider loss of product when the DG method is used within the recommended 45-min experimental period.

When, however, the DG method was adapted for human use with [^{18}F]fluorodeoxyglucose (FDG) and positron emission tomography (PET), prolonged scanning times well beyond 45 min were at first required because of the slowness of the scanning procedure. After 120 min following a pulse of FDG, total tissue activity was observed to decline, indicating loss of product (Phelps et al., 1979). The kinetic model of the DG method was therefore modified for use with long experimental periods by the addition of a first-order rate constant for the dephosphorylation of [^{18}F]fluorodeoxyglucose-6-phosphate (Phelps et al., 1979). This model contains two compartments and four rate constants (4K model) and includes the arbitrary assumption that beginning at zero time a constant fraction of the total product recycles back to the precursor pool per unit time, the so-called k_4^*. With newer, multiplane, and more sensitive PET scanners, many scans can now be completed in a shorter time period, e.g., within 45–60 min following the pulse of FDG. Despite the lack of evidence for loss of [^{18}F]fluorodeoxyglucose-6-phosphate in this time interval, however, the 4K model continues to be widely used in shorter-duration studies. The main justification for the use of the 4K model appears to be the better nonlinear, least-squares fit of the time course of total tissue radioactivity with the 4K than with the 3K model. Analyses of model-related errors, including the sensitivity of calculated glucose utilization to values of the rate constants and differences in glucose utilization calculated with alternative formulas, have been based on the assumption that this model that incorporates first-order dephosphorylation of [^{18}F]fluorodeoxyglucose-6-phosphate most closely describes the true kinetics of FDG in brain tissue.

Nelson and co-workers (1987) have shown that a kinetic model designed for a homogeneous tissue with a unique set of time-invariant rate constants cannot be used to characterize the kinetic behavior of DG in a heterogeneous tissue. We have recently reported that in freeze-blown whole brain, the tissue heterogeneity alone can account for the appearance of a rate constant for dephosphorylation, i.e., k_4^*, exceeding one-tenth the value of the phosphorylation rate constant in the first 45 min following a pulse of DG when the 4K model is used (Schmidt et al., 1989*b*). In the present study, we examine the effects of tissue heterogeneity on the choice of a kinetic model for the DG method and the effect that the model configuration exerts on the calculated regional CMR_{glc} ($rCMR_{glc}$). The results of the current study demonstrate that the use of the 4K model in a heterogeneous tissue leads to an estimate of the rate constant for dephosphorylation greater than zero even in the absence of product loss and a significant overestimation of $rCMR_{glc}$.

THEORY

Definition of heterogeneous tissue

A schematic representation of a heterogeneous tissue is illustrated in Fig. 1A. The heterogeneous tissue is assumed to consist of n smaller homogeneous subregions. C_{e1}^*, C_{e2}^*, . . . , C_{en}^* represent the DG concentrations in each homogeneous subregion of the mixed brain tissue, and C_{m1}^*, C_{m2}^*, . . . , C_{mn}^* represent the concentrations of DG-6-P (and all metabolites derived from DG-6-P) in these same subregions, respectively. K_{11}^*, K_{12}^*, . . . , K_{1n}^* and k_{21}^*, k_{22}^*, . . . , k_{2n}^* are the corresponding rate constants for transport of DG from plasma to brain tissue and from brain to plasma, respectively. k_{31}^*, k_{32}^*, . . . , k_{3n}^* are the rate constants for phosphorylation of DG in the tissues to DG-6-P. C_p^* represents the DG concentration in the arterial plasma. The following set of equations describes the rate of change in concentration of DG in each of the homogeneous subregions of the mixed tissue:

$$\begin{aligned}
\frac{dC_{e1}^*}{dt}(t) &= K_{11}^* C_p^*(t) - (k_{21}^* + k_{31}^*) C_{e1}^*(t) \\
\frac{dC_{e2}^*}{dt}(t) &= K_{12}^* C_p^*(t) - (k_{22}^* + k_{32}^*) C_{e2}^*(t) \\
&\vdots \\
\frac{dC_{en}^*}{dt}(t) &= K_{1n}^* C_p^*(t) - (k_{2n}^* + k_{3n}^*) C_{en}^*(t)
\end{aligned} \tag{1}$$

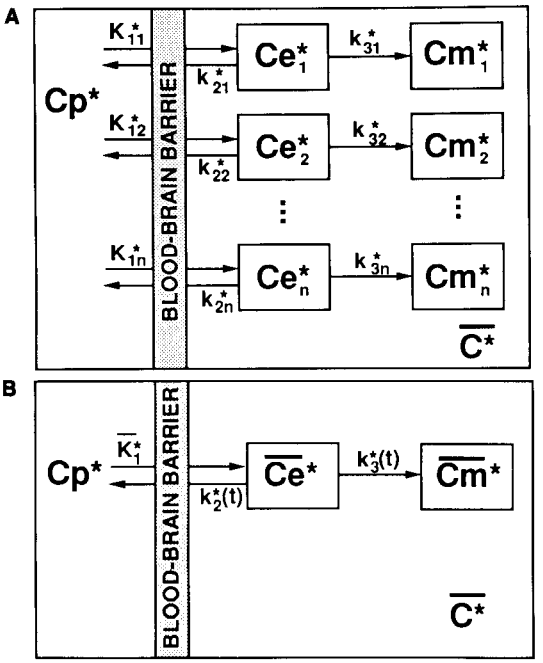

FIG. 1. Schematic diagram of heterogeneous tissue. **A:** Representation of the heterogeneous tissue as an aggregation of n smaller homogeneous subregions. C^*_p represents the deoxyglucose (DG) concentration in the arterial plasma. C^*_{e1}, C^*_{e2}, . . . , C^*_{en} represent the DG concentrations in the exchangeable pool of each homogeneous subregion of the mixed brain tissue, and C^*_{m1}, C^*_{m2}, . . . , C^*_{mn} represent the concentrations of deoxyglucose-6-phosphate (DG-6-P) and all metabolites derived from DG-6-P. K^*_{11}, K^*_{12}, . . . , K^*_{1n} and k^*_{21}, k^*_{22}, . . . , k^*_{2n} are the rate constants for carrier-mediated transport of DG from plasma to brain tissue and from brain to plasma, respectively. k^*_{31}, k^*_{32}, . . . , k^*_{3n} are the rate constants for phosphorylation by hexokinase of DG in the tissue to DG-6-P. $\overline{C}^*$ represents the concentration of total radioactivity in the mixed tissue. **B:** Tissue heterogeneity model. The rate "constants" in the model are represented by the following: $\overline{K}^*_1$, the rate constant for transport of DG into the mixed tissue; $k^*_2(t)$, the time-varying effective rate constant at time t for transport of DG from brain tissue to plasma; and $k^*_3(t)$, the time-varying effective rate constant at time t for phosphorylation of DG in the tissue. $\overline{K}^*_1$ is the mass-weighted average of K^*_{11}, K^*_{12}, . . . , K^*_{1n}, the inward transport rate constants for each of the homogeneous subregions. The effective rate constants for efflux and phosphorylation are the averages of the rate constants for outward transport and phosphorylation, respectively, weighted by the tissue free DG concentration in each of the subregions. In the model, $k^*_2(t)$ and $k^*_3(t)$ are approximated by declining exponential functions. $\overline{C}^*_e$ and $\overline{C}^*_m$ are the mass-weighted tissue concentrations of DG and DG-6-P, respectively.

If the relative mass weights of each of the homogeneous subregions are w_1, w_2, . . . , w_n, where $\Sigma_{j=1}^n w_j = 1.0$, then the total change in DG concentration in the mixed tissue as a whole is found by summing the changes in DG concentration in each subregion weighted by its relative tissue mass, i.e.,

$$\frac{d\overline{C}^*_e}{dt}(t) = \sum_{j=1}^{n} w_j \frac{dC^*_{ej}}{dt}(t) = \left(\sum_{j=1}^{n} w_j K^*_{1j}\right) C^*_p(t) - \left[\sum_{j=1}^{n} w_j (k^*_{2j} + k^*_{3j}) C^*_{ej}(t)\right] \quad (2)$$

where $\overline{C}^*_e(t)$ represents the mass-weighted average DG concentration in the heterogeneous tissue at any time t. Let $\overline{K}^*_1$ be defined by

$$\overline{K}^*_1 = \sum_{j=1}^{n} w_j K^*_{1j} \quad (3)$$

$\overline{K}^*_1$, the rate constant for transport of DG into the mixed tissue, is the mass-weighted average of the inward transport rate constants of each of the subregions. Thus,

$$\frac{d\overline{C}^*_e}{dt}(t) = \overline{K}^*_1 C^*_p(t) - \left[\sum_{j=1}^{n} w_j (k^*_{2j} + k^*_{3j}) C^*_{ej}(t)\right] \quad (4)$$

Multiplying the last term of Eq. 4 by

$$1.0 = \frac{\sum_{j=1}^{n} w_j C^*_{ej}(t)}{\sum_{j=1}^{n} w_j C^*_{ej}(t)} = \frac{\overline{C}^*_e(t)}{\sum_{j=1}^{n} w_j C^*_{ej}(t)}$$

yields

$$\frac{d\overline{C}^*_e}{dt}(t) = \overline{K}^*_1 C^*_p(t) - \frac{\left[\sum_{j=1}^{n} w_j (k^*_{2j} + k^*_{3j}) C^*_{ej}(t)\right]}{\left[\sum_{j=1}^{n} w_j C^*_{ej}(t)\right]} \overline{C}^*_e(t) \quad (5)$$

The effective rate constant at any time t for outward transport of DG from the heterogeneous tissue to the plasma, $k^*_2(t)$, is the instantaneous rate of efflux of DG from the mixed tissue divided by the tissue DG pool size, i.e.,

$$\text{effective } k^*_2(t) = \frac{\sum_{j=1}^{n} w_j k^*_{2j} C^*_{ej}(t)}{\sum_{j=1}^{n} w_j C^*_{ej}(t)} \quad (6)$$

Similarly, $k_3^*(t)$, the effective rate constant at time t for phosphorylation of DG to DG-6-P in the heterogeneous tissue, is the instantaneous rate of phosphorylation of DG in the mixed tissue divided by the precursor pool size, i.e., the mass-weighted average DG concentration:

$$\text{effective } k_3^*(t) = \frac{\sum_{j=1}^{n} w_j k_{3j}^* C_{ej}^*(t)}{\sum_{j=1}^{n} w_j C_{ej}^*(t)} \quad (7)$$

Substitution of Eqs. 6 and 7 into Eq. 5 gives

$$\frac{d\overline{C}_e^*}{dt}(t) = \overline{K}_1^* C_p^* - [k_2^*(t) + k_3^*(t)]\overline{C}_e^*(t) \quad (8)$$

The effective rate constants for the efflux and phosphorylation are the averages of the rate constants for outward transport and phosphorylation, respectively, weighted by the tissue free DG concentration in each of the subregions. Because the time course of the DG concentration in each constituent tissue of the mixture is different, the effective rate constants for efflux and phosphorylation of DG in the heterogeneous tissue as a whole vary with time as the relative weight of each subregion varies with time. Initially, the effective rate constants for efflux and phosphorylation of DG in the heterogeneous tissue reflect mainly the subregions with the highest rates of blood flow and transport, i.e.,

$$\lim_{t\to 0} k_2^*(t) = \frac{\sum_{j=1}^{n} w_j K_{1j}^* k_{2j}^*}{\sum_{j=1}^{n} w_j K_{1j}^*} = \frac{\sum_{j=1}^{n} w_j K_{1j}^* k_{2j}^*}{\overline{K}_1^*} \quad (9)$$

and

$$\lim_{t\to 0} k_3^*(t) = \frac{\sum_{j=1}^{n} w_j K_{1j}^* k_{3j}^*}{\sum_{j=1}^{n} w_j K_{1j}^*} = \frac{\sum_{j=1}^{n} w_j K_{1j}^* k_{3j}^*}{\overline{K}_1^*} \quad (10)$$

With increasing time after a pulse, as the various subregions and the plasma come into steady state, but before loss of product becomes significant, $dC_{ej}^*(t)/dt \approx 0$, and

$$C_{ej}^*(t) \text{ (steady state)} \approx \frac{K_{1j}^*}{k_{2j}^* + k_{3j}^*} C_p^*(t) \quad (11)$$

The effective rate constants for outward transport and phosphorylation then approach the averages for the heterogeneous tissue as a whole, weighted by the tissue distribution space and mass, as follows:

$$k_2^*(t) \text{ (steady state)} \approx \frac{\sum_{j=1}^{n} w_j[K_{1j}^*/(k_{2j}^* + k_{3j}^*)]k_{2j}^*}{\sum_{j=1}^{n} w_j[K_{1j}^*/(k_{2j}^* + k_{3j}^*)]} \quad (12)$$

and

$$k_3^*(t) \text{ (steady state)} \approx \frac{\sum_{j=1}^{n} w_j[K_{1j}^*/(k_{2j}^* + k_{3j}^*)]k_{3j}^*}{\sum_{j=1}^{n} w_j[K_{1j}^*/(k_{2j}^* + k_{3j}^*)]} \quad (13)$$

The rates of change of DG-6-P in each of the subregions of the mixed tissue are given by

$$\begin{aligned} \frac{dC_{m1}^*}{dt}(t) &= k_{31}^* C_{e1}^*(t) \\ \frac{dC_{m2}^*}{dt}(t) &= k_{32}^* C_{e2}^*(t) \\ &\cdot \\ &\cdot \\ &\cdot \\ \frac{dC_{mn}^*}{dt}(t) &= k_{3n}^* C_{en}^*(t) \end{aligned} \quad (14)$$

and the rate of change of DG-6-P for the mixed region as a whole is

$$\frac{d\overline{C}_m^*}{dt}(t) = k_3^*(t)\overline{C}_e^*(t) \quad (15)$$

where $\overline{C}_m^*(t)$ represents the mass-weighted average DG-6-P concentration in the heterogeneous tissue at time t and $k_3^*(t)$ is as defined in Eq. 7.

The total concentration of radioactivity in the mixed tissue, $\overline{C}^*(t)$, is the sum of the concentrations of DG and DG-6-P, i.e.,

$$\overline{C}^*(t) = \overline{C}_e^*(t) + \overline{C}_m^*(t) \quad (16)$$

where $\overline{C}_e^*(t)$ and $\overline{C}_m^*(t)$ are the solutions to Eqs. 8

and 15 with the initial conditions that $\bar{C}^*_e(0) = 0$ and $\bar{C}^*_m(0) = 0$.

Description of model for heterogeneous tissue

If $C^*_p(t)$ and the parameters n, w_1 through w_n, K^*_{11} through K^*_{1n}, k^*_{21} through k^*_{2n}, and k^*_{31} through k^*_{3n} were known, then Eqs. 8, 15, and 16 could be used to estimate the concentrations of DG, DG-6-P, and total tissue activity in the brain. The large number ($4 \times n$) of unknown parameters used to describe the heterogeneous tissue, however, makes determination of these parameters for a particular set of experimental data impractical. The time-varying nature of the effective rate constants for efflux and phosphorylation, $k^*_2(t)$ and $k^*_3(t)$, can, however, be reasonably well approximated by exponential functions that decline to the mass-weighted averages $\bar{k}^*_2$ and $\bar{k}^*_3$, as will be seen from the simulation experiments below. Furthermore, if the ratio k^*_{2j}/k^*_{3j} is approximately the same for each of the homogeneous subregions, then the same exponential function (but with a different scaling factor) can be used to describe both $k^*_2(t)$ and $k^*_3(t)$. The equations describing the rates of change in DG and DG-6-P in the mixed tissue as a whole are therefore

$$\frac{d\bar{C}^*_e}{dt}(t) = \bar{K}^*_1 C^*_p - [k^*_2(t) + k^*_3(t)]\bar{C}^*_e(t) \quad (17)$$

$$\frac{d\bar{C}^*_m}{dt}(t) = k^*_3(t)\bar{C}^*_e(t) \quad (18)$$

where

$$k^*_2(t) = \bar{k}^*_2(1.0 + \alpha e^{-\beta t}) \quad (19)$$

and

$$k^*_3(t) = \bar{k}^*_3(1.0 + \alpha e^{-\beta t}) \quad (20)$$

Using exponential approximations for $k^*_2(t)$ and $k^*_3(t)$ reduces the number of parameters to five: $\bar{K}^*_1$, the mass-weighted influx rate constant; $\bar{k}^*_2$ and $\bar{k}^*_3$, the mass- and distribution space–weighted rate constants for efflux and phosphorylation, respectively; and α and β, the parameters that describe the time-varying nature of $k^*_2(t)$ and $k^*_3(t)$. These parameters may be estimated by nonlinear least-squares fitting routines. Equations 17 through 20 constitute the tissue heterogeneity model, which is illustrated in Fig. 1B.

$rCMR_{glc}$ in heterogeneous tissue

For each subregion j of the mixed tissue, the rate of glucose utilization in the absence of product loss is as follows (Sokoloff et al., 1977):

$$R_j = \frac{C^*_j(T) - C^*_{ej}(T)}{LC\left\{\int_0^T [C^*_p(t)/C_p]dt - \int_0^T [C^*_p(t)/C_p]e^{-(k^*_{2j}+k^*_{3j})(T-t)}dt\right\}} \quad (21)$$

where $C^*_j(T)$ is the measured total tissue activity in subregion j at time T, the final time of the study; $C^*_{ej}(T)$ is the estimated concentration of DG in subregion j; k^*_{2j} and k^*_{3j} are the rate constants for efflux of DG from tissue to plasma and for phosphorylation of DG to DG-6-P in the jth tissue, respectively; LC is the lumped constant and is assumed to be equal for all subregions; and $C^*_p(t)$ and C_p are the arterial plasma DG and glucose concentrations, respectively. Following a pulse of DG, the first term in the denominator of Eq. 21 increases with time while the second term decreases. By 45 min following the pulse of DG, the second term in the denominator becomes negligible compared with the term from which it is being subtracted. Thus,

$$R_j \approx \frac{C^*_j(T) - C^*_{ej}(T)}{LC\int_0^T [C^*_p(t)/C_p]dt} \quad (22)$$

and the weighted average glucose utilization for a heterogeneous tissue, $\bar{R}$, is calculated by

$$\bar{R} = \sum_{j=1}^{n} w_j R_j \approx \frac{\sum_{j=1}^{n} w_j C^*_j(T) - \sum_{j=1}^{n} w_j C^*_{ej}(T)}{LC\int_0^T [C^*_p(t)/C_p]dt} = \frac{\bar{C}^*(T) - \bar{C}^*_e(T)}{LC\int_0^T [C^*_p(t)/C_p]dt} \quad (23)$$

where $\bar{C}^*(T)$ is the concentration of radioactivity actually measured in the mixed tissue at time T, $\bar{C}^*_e(T)$ is the estimated concentration of DG in the mixed tissue, and LC, C^*_p, and C_p are as defined above.

METHODS

In the current study the time courses of the concentrations of DG, DG-6-P, and total radioactivity in a hypothetical tissue consisting of gray and white matter were simulated for 45 min following a pulse of DG. No loss of DG-6-P from any tissue during this time period was assumed. The mixed tissue was assumed to consist of two

homogeneous tissues (gray and white) in proportions ranging from 100% gray/0% white to 0% gray/100% white in 10% increments. The rate constants for the white matter were representative of those estimated in several white matter structures in the rat ($K_1^* = 0.085$ ml/g/min, $k_2^* = 0.135$ min^{-1}, and $k_3^* = 0.02$ min^{-1}) (Sokoloff et al., 1977). As the influx and efflux rate constants reflect the rate of blood flow, gray matter values for K_1^* and k_2^* were chosen to be four times those in white matter to coincide with the four-to-one ratio of blood flow found in the gray and white matter structures of the rat (Sakurada et al., 1978). Coupling of rates of blood flow and metabolism, at least under normal physiological conditions, led to the choice of a value of k_3^* in gray matter also four times the corresponding value in white matter. Gray matter rate constants used in the simulation study were therefore $K_1^* = 0.34$ ml/g/min, $k_2^* = 0.54$ min^{-1}, and $k_3^* = 0.08$ min^{-1}. In addition, a mixed tissue comprising 50% gray and 50% white matter, with both gray and white regions consisting of three homogeneous subregions representing a distribution of high (50% above average), average, and low (50% below average) rates of blood flow and metabolism for gray and white matter, was simulated. The rate constants and weighting factors used in the simulated mixed tissues are summarized in Table 1. A typical experimentally determined arterial plasma time course of $C_p^*(t)$ following a pulse of DG was used as the input function. The time courses of DG and DG-6-P concentrations were calculated for the homogeneous gray and white matter regions according to Eqs. 1 and 14, and the mass-weighted averages for the mixed tissues computed. The mass-weighted average total tissue activity was then calculated by Eq. 16. The mass-weighted average concentrations of DG, DG-6-P, and total tissue activity were sampled at 12 time points, i.e., at 1, 2.5, 5, 7, 10, 15, 20, 25, 30, 35, 40, and 45 min following the pulse of DG. These data points represent the "measured" tissue concentrations in each of the mixed tissues without measurement errors. For each mixed tissue a nonlinear least-squares procedure, according to the Levenberg-Marquardt method (Press et al., 1986), was used to estimate the rate constants for the usual two homogeneous tissue models, i.e., the 3K (no loss) and the 4K (loss) models, and for the tissue heterogeneity model from either the DG and DG-6-P concentrations or from the total tissue activity data. The model-predicted time courses of DG and DG-6-P concentrations, as well as their partial derivatives with respect to each of the model parameters, were required by the nonlinear least-squares fitting procedure and were determined by numerical solution of the model differential equations by a fourth-order Runge-Kutta procedure with adaptive stepsize control (Press et al., 1986).

Tests for goodness of fit

To test whether the fit of the data by the 4K model was significantly better than that of the 3K model, and whether the fit of the tissue heterogeneity model was significantly better than that of the 3K model, an F test for comparison of nested models was used (Landlaw and DiStefano, 1984). The F value was computed as

$$F = \frac{(\mathrm{WRSS}_1 - \mathrm{WRSS}_2)/(df_1 - df_2)}{(\mathrm{WRSS}_2/df_2)} \quad (24)$$

where WRSS_1 and WRSS_2 are the weighted residual sums of squares computed by use of the 3K (model 1) and either the 4K or the tissue heterogeneity model (model 2), and df_1 and df_2 are the corresponding degrees of freedom. To compare the goodness of fit of the nonnested 4K and tissue heterogeneity models, both the Akaike information criterion (AIC) and the Schwarz criterion (SC) were used (Landlaw and DiStefano, 1984). For each model, the Akaike information criterion was computed as

$$\mathrm{AIC} = N \ln(\mathrm{WRSS}) + (2)(P) \quad (25)$$

where N is the number of data points, P is the number of parameters in the model, and WRSS is as defined above. The Schwarz criterion for each model was computed as

$$\mathrm{SC} = \mathrm{WRSS} + P \ln(N) \quad (26)$$

TABLE 1. *Heterogeneous tissue used in simulation studies*

Rate constants used to simulate homogeneous tissue subregions

	Subregion					
	High gray	Moderate gray	Low gray	High white	Moderate white	Low white
K_1^* (ml/g/min)	0.5100	0.3400	0.1700	0.1275	0.0850	0.0425
k_2^* (min^{-1})	0.8100	0.5400	0.2700	0.2025	0.1350	0.0675
k_3^* (min^{-1})	0.1200	0.0800	0.0400	0.0300	0.0200	0.0100

Composition of heterogeneous tissue regions

	Simulation no.											
	1	2	3	4	5	6	7	8	9	10	11	12
% high gray												10
% moderate gray	100	90	80	70	60	50	40	30	20	10	0	30
% low gray												10
% high white												10
% moderate white	0	10	20	30	40	50	60	70	80	90	100	30
% low white												10

True mass-weighted influx rate constant and mass- and distribution space–weighted efflux and phosphorylation rate constants for heterogeneous tissue regions

$\bar{K}_1^*$ (ml/g/min)	0.3400	0.3145	0.2890	0.2635	0.2380	0.2125	0.1870	0.1615	0.1360	0.1105	0.0805	0.2125
$\bar{k}_2^*$ (min^{-1})	0.5400	0.4995	0.4590	0.4185	0.3780	0.3375	0.2970	0.2565	0.2160	0.1755	0.1350	0.3375
$\bar{k}_3^*$ (min^{-1})	0.0800	0.0740	0.0680	0.0620	0.0560	0.0500	0.0440	0.0380	0.0320	0.0260	0.0200	0.0500

The model with the smallest Akaike information or Schwarz criterion is considered to best fit the data with the fewest number of parameters.

Calculation of $rCMR_{glc}$

To evaluate the influence of the choice of kinetic model on the calculated metabolic rate for glucose, $rCMR_{glc}$ was calculated as follows for each mixed tissue and for each of the three models with two sets of rate constants: the rate constants estimated from the time course of both the DG and the DG-6-P concentrations for the current simulation data and the rate constants estimated from the total tissue activity-time course for the current simulation data:

3K model

The equation used for calculation of $rCMR_{glc}$ is that of Sokoloff et al. (1977):

$$rCMR_{glc} = \frac{\overline{C}^*(T)^{measured} - \hat{K}_1^* \int_0^T C_p^*(t) e^{-(\hat{k}_2^* + \hat{k}_3^*)(T-t)} dt}{LC \left\{ \int_0^T [C_p^*(t)/C_p] dt - \int_0^T [C_p^*(t)/C_p] e^{-(\hat{k}_2^* + \hat{k}_3^*)(T-t)} dt \right\}} \quad (27)$$

where $\overline{C}^*(T)$ is the "measured" mass-weighted average total tissue activity at time T, the final time of the study; $\hat{K}_1^*$, $\hat{k}_2^*$, and $\hat{k}_3^*$ are the rate constants for transport of DG from plasma to tissue, for efflux of DG from tissue to plasma, and for phosphorylation of DG to DG-6-P in the tissue estimated from the 3K model, respectively; LC is the lumped constant; and $C_p^*(t)$ and C_p are the arterial plasma DG and glucose concentrations, respectively. In this simulation study, C_p is assumed to be 140 mg/dl and $LC = 0.48$ (Sokoloff et al., 1977).

4K model

$rCMR_{glc}$ was calculated by the equation derived by Phelps et al. (1979) as follows:

$$rCMR_{glc} = \frac{\overline{C}^*(T)^{measured} - C_e^*(T)^{estimated}}{C_m^*(T)^{estimated}} \left(\frac{\hat{K}_1^* \hat{k}_3^*}{\hat{k}_2^* + \hat{k}_3^*} \right) \frac{C_p}{LC} \quad (28)$$

where $\overline{C}^*(T)$, C_p, and LC are as defined above; $\hat{K}_1^*$, $\hat{k}_2^*$, and $\hat{k}_3^*$ are the rate constants estimated from the 4K model; and $C_e^*(T)^{estimated}$ and $C_m^*(T)^{estimated}$ are the concentrations of DG and DG-6-P, respectively, in the tissue at time T predicted by the 4K model. Although the estimate of the rate constant for dephosphorylation, k_4^*, does not appear explicitly in Eq. 28, it has been incorporated into the computation of $C_e^*(T)^{estimated}$ and $C_m^*(T)^{estimated}$.

Tissue heterogeneity model

As derived in Eq. 23, $rCMR_{glc}$ is given by

$$rCMR_{glc} = \frac{\overline{C}^*(T)^{measured} - \overline{C}_e^*(T)^{estimated}}{LC \int_o^T [C_p^*(t)/C_p] dt} \quad (29)$$

For calculation of $rCMR_{glc}$ the values of $C_e^*(T)^{estimated}$, $C_m^*(T)^{estimated}$, and $\overline{C}_e^*(T)^{estimated}$, (Eqs. 28 and 29) were found by numerical solution of the appropriate model differential equations by a fourth-order Runge-Kutta procedure with adaptive stepsize control (Press et al., 1986).

RESULTS

Simulation data

Figure 2 illustrates the time courses of the concentrations of DG, DG-6-P, and total tissue radioactivity following a pulse of DG in a heterogeneous tissue consisting of 50% homogeneous gray and 50% homogeneous white matter. The resultant time courses of the effective rate constants for efflux of DG from the mixed and for phosphorylation of DG in the mixed tissue, $k_2^*(t)$ and $k_3^*(t)$, calculated by Eqs. 6 and 7, are illustrated in Fig. 3. Note that the curve is the same for both effective rate constants; they differ only by a scaling factor.

Values of rate constants

The least-squares best-fit estimates of the rate constants for the 3K, 4K, and tissue heterogeneity models for the simulated heterogeneous tissue are shown in Tables 2 and 3. When the DG and DG-6-P concentrations were used to estimate the rate constants, the fits of both the 4K and the tissue heterogeneity models to the data were statistically significantly better than the fit of the 3K model ($p < 0.005$), and the fit of the tissue heterogeneity model was better than that of the 4K model according to both the Akaike and Schwarz criteria in all heterogeneous tissues. When total tissue activity was used to estimate the rate constants, the fit of the 4K model to the data was better than the fit of the 3K model at the $p < 0.05$ level, the fit of the tissue heterogeneity model was better than that of the 3K model at the $p < 0.005$ level, and the fit of the tissue heterogeneity model was better than that of the 4K model according to both the Akaike and the Schwarz criteria. The estimated values $\hat{K}_1^*$ for the 3K and 4K models and $\hat{K}_1^*$ for the tissue heterogeneity model all tended to overestimate the true mass-weighted average for the mixed tissue, although by <15%. The estimated values $\hat{k}_2^*$ and $\hat{k}_2^*$ similarly tended to overestimate slightly the true weighted average efflux rate constant for the heterogeneous tissue. The estimate $\hat{k}_3^*$ is higher for the 4K model than for the 3K model due to the assumed presence of dephosphorylation in the 4K model; with the 4K model the estimate $\hat{k}_4^*$ was between 1 and 27% of the value of $\hat{k}_3^*$ for the mixed tissue even though the true rate constant for dephosphorylation is zero (Fig. 4). Regardless of whether total tissue activity or the DG and DG-6-P concentrations were used for the estimation of the rate

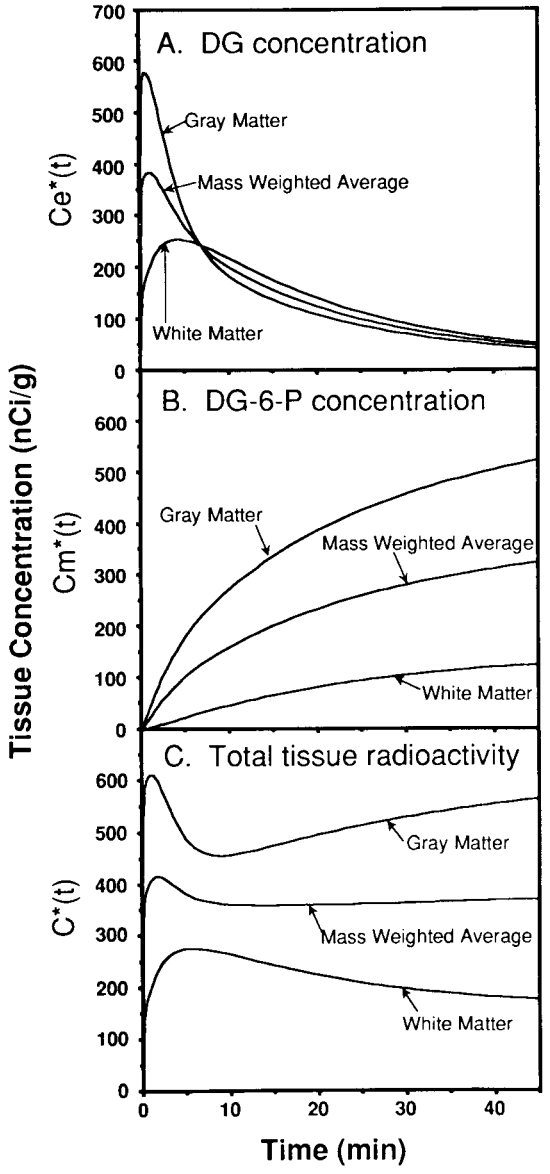

FIG. 2. Representative data used in the simulation studies. **A:** The tissue deoxyglucose (DG) concentration in gray matter, white matter, and mass-weighted average DG concentration in a hypothetical mixed brain tissue consisting of 50% gray and 50% white matter following a pulse of DG. **B and C:** The tissue deoxyglucose-6-phosphate (DG-6-P) concentrations and total tissue activity in the same hypothetical gray, white, and mixed tissues. The time courses of DG and DG-6-P were calculated for the homogeneous gray and white matter regions, and the mass-weighted averages for the hypothetical mixture determined. Total tissue activity was found by summing the DG and DG-6-P activities. The mass-weighted average DG, DG-6-P, and total tissue activities were sampled at 12 time points, i.e., at 1, 2.5, 5, 7, 10, 15, 20, 25, 30, 35, 40, and 45 min following the pulse of DG. For the simulation study, these data points represent the "measured" tissue concentrations in each of the mixed tissues.

constants, the estimate $\hat{k}_4^*$ in the 4K model increased relative to the value of $\hat{k}_3^*$ as the proportion of white matter in the heterogeneous mixed tissue increased.

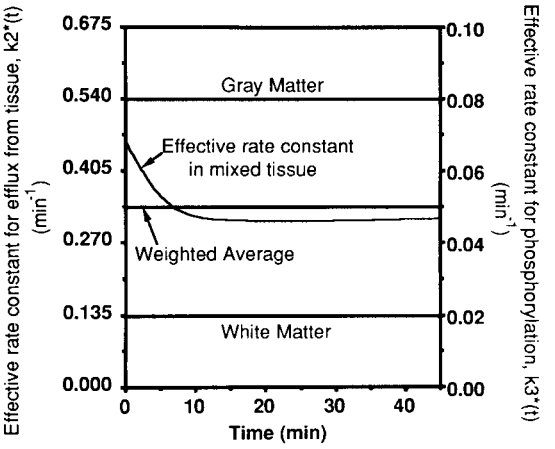

FIG. 3. Time-varying effective rate constants for transport of deoxyglucose (DG) from the mixed brain tissue to the plasma, $k_2^*(t)$, and for phosphorylation of DG in the tissue to deoxyglucose-6-phosphate (DG-6-P), $k_3^*(t)$, for the mixed tissue consisting of 50% gray and 50% white matter. $k_2^*(t)$ and $k_3^*(t)$ are the averages of the rate constants for outward transport and phosphorylation, respectively, weighted by the tissue free DG concentration in each of the subregions. Because the time course of the DG concentration in each constituent tissue of the mixture is different, the effective rate constants for efflux and phosphorylation of DG in the heterogeneous tissue as a whole vary with time as the relative weight of each subregion varies with time. Furthermore, if the ratio k_{2j}^*/k_{3j}^* is the same for each of the homogeneous subregions, then the time courses of $k_2^*(t)$ and $k_3^*(t)$ differ only by a scaling factor. In the tissue heterogeneity model, $k_2^*(t)$ and $k_3^*(t)$ were approximated by appropriately scaled declining exponential functions.

Time courses of DG, DG-6-P, and total tissue radioactivity concentrations

Figure 5A illustrates the time courses of the tissue concentrations of DG and DG-6-P (50% gray and 50% white matter) predicted by each of the three models when the rate constants estimated from the DG and DG-6-P data were used. For both the 3K and the 4K models, the concentration of DG in the tissue is overestimated early in the time course and underestimated at later times. DG-6-P concentrations are accurately predicted for the first 10 min and overestimated from ~15 to 25 min. With the 3K model a slight overestimation of DG-6-P continues to the end of the experimental period at 45 min, but in the model that assumes loss of product, DG-6-P is underestimated between 35 and 45 min. The tissue heterogeneity model accurately predicts the time courses of DG and DG-6-P concentrations. The same patterns of overestimation/underestimation were observed in all simulations, with the magnitude of the difference between the model predictions and the "measured" data increasing as the proportion of white matter in the mixed tissue increased.

Time courses of tissue concentration of DG, DG-6-P, and total tissue activity predicted by each of

TABLE 2. *Rate constants estimated from deoxyglucose and deoxyglucose-6-phosphate concentrations in simulated heterogeneous tissue*

	Simulation no.											
	1	2	3	4	5	6	7	8	9	10	11	12
3K model												
$\hat{K}_1^*$ (ml/g/min)	0.3830	0.3591	0.3314	0.3000	0.2675	0.2336	0.2006	0.1712	0.1438	0.1188	0.0919	0.2290
$\hat{}$ SE	0.0027	0.0063	0.0118	0.0155	0.0174	0.0174	0.0160	0.0137	0.0105	0.0066	0.0006	0.0203
$\hat{k}_2^*$ (min^{-1})	0.6091	0.5698	0.5255	0.4760	0.4249	0.3710	0.3181	0.2715	0.2277	0.1880	0.1451	0.3648
$\hat{}$ SE	0.0046	0.0108	0.0204	0.0269	0.0303	0.0307	0.0286	0.0247	0.0191	0.0119	0.0010	0.0363
$\hat{k}_3^*$ (min^{-1})	0.0806	0.0745	0.0687	0.0631	0.0576	0.0520	0.0463	0.0403	0.0340	0.0273	0.0200	0.0527
SE	0.0002	0.0006	0.0011	0.0015	0.0018	0.0020	0.0020	0.0019	0.0015	0.0010	0.0001	0.0024
WRSS	8.9 $\times 10^{-4}$	6.1 $\times 10^{-3}$	2.8 $\times 10^{-2}$	6.5 $\times 10^{-2}$	1.1 $\times 10^{-1}$	1.7 $\times 10^{-1}$	2.2 $\times 10^{-1}$	2.4 $\times 10^{-1}$	2.4 $\times 10^{-1}$	1.6 $\times 10^{-1}$	2.4 $\times 10^{-3}$	2.4 $\times 10^{-1}$
4K model												
$\hat{K}_1^*$ (ml/g/min)	0.3834	0.3499	0.3139	0.2782	0.2430	0.2104	0.1812	0.1557	0.1329	0.1123	0.0915	0.2017
$\hat{}$ SE	0.0031	0.0057	0.0102	0.0128	0.0135	0.0130	0.0117	0.0099	0.0077	0.0051	0.0006	0.0141
$\hat{k}_2^*$ (min^{-1})	0.6096	0.5565	0.5000	0.4440	0.3887	0.3370	0.2906	0.2497	0.2130	0.1795	0.1446	0.3240
$\hat{}$ SE	0.0052	0.0094	0.0171	0.0214	0.0229	0.0223	0.0202	0.0173	0.0135	0.0088	0.0010	0.0244
$\hat{k}_3^*$ (min^{-1})	0.0805	0.0765	0.0728	0.0689	0.0647	0.0600	0.0545	0.0479	0.0402	0.0311	0.0202	0.0631
$\hat{}$ SE	0.0004	0.0008	0.0016	0.0022	0.0026	0.0029	0.0029	0.0027	0.0022	0.0014	0.0001	0.0035
$\hat{k}_4^*$ (min^{-1})	−0.0001	0.0013	0.0029	0.0046	0.0064	0.0080	0.0094	0.0103	0.0103	0.0083	0.0006	0.0102
SE	0.0002	0.0004	0.0009	0.0014	0.0018	0.0022	0.0025	0.0027	0.0027	0.0022	0.0003	0.0026
WRSS	8.9 $\times 10^{-4}$	4.0 $\times 10^{-3*}$	1.8 $\times 10^{-2*}$	4.1 $\times 10^{-2*}$	6.9 $\times 10^{-2*}$	9.8 $\times 10^{-2*}$	1.2 $\times 10^{-1*}$	1.4 $\times 10^{-1*}$	1.3 $\times 10^{-1*}$	9.0 $\times 10^{-2*}$	2.0 $\times 10^{-3}$	1.3 $\times 10^{-1*}$
Tissue heterogeneity model												
$\hat{K}_1^*$ (ml/g/min)	—	0.3547	0.3271	0.2977	0.2674	0.2381	0.2081	0.1792	0.1507	0.1216	—	0.2380
$\hat{}$ SE		0.0012	0.0031	0.0048	0.0036	0.0028	0.0015	0.0008	0.0011	0.0008		0.0049
$\hat{k}_2^*$ (min^{-1})	—	0.5543	0.5064	0.4560	0.4025	0.3539	0.3057	0.2612	0.2202	0.1817	—	0.3460
$\hat{}$ SE		0.0022	0.0051	0.0078	0.0059	0.0045	0.0024	0.0013	0.0017	0.0013		0.0077
$\hat{k}_3^*$ (min^{-1})	—	0.0732	0.0665	0.0600	0.0533	0.0470	0.0408	0.0349	0.0294	0.0245	—	0.0468
$\hat{}$ SE		0.0002	0.0005	0.0007	0.0006	0.0005	0.0003	0.0002	0.0003	0.0002		0.0009
$\hat{\alpha}$ (min^{-1})	—	0.0964	0.2249	0.3533	0.4438	0.5615	0.6761	0.7353	0.7217	0.5709	—	0.6980
$\hat{}$ SE		0.0051	0.0158	0.0295	0.0267	0.0257	0.0177	0.0126	0.0211	0.0187		0.0469
$\hat{\beta}$ (min^{-1})	—	0.3246	0.4575	0.4732	0.3823	0.3590	0.3336	0.3042	0.2862	0.3013	—	0.3720
SE		0.0250	0.0416	0.0502	0.0298	0.0213	0.0114	0.0070	0.0117	0.0152		0.0314
WRSS	—	1.9 $\times 10^{-4*,‡}$	1.4 $\times 10^{-3*,‡}$	4.2 $\times 10^{-3*,‡}$	3.2 $\times 10^{-3*,‡}$	2.6 $\times 10^{-3*,‡}$	1.1 $\times 10^{-3*,‡}$	5.2 $\times 10^{-4*,‡}$	1.5 $\times 10^{-3*,‡}$	1.4 $\times 10^{-3*,‡}$	—	7.8 $\times 10^{-3*,‡}$

Values are estimates ± standard errors of the estimate; WRSS, weighted sum of squares of the residuals.
* Statistically significant improvement in fit over 3K model (F test, $p < 0.005$).
‡ Improvement in fit over 4K model (by the Akaike and Schwarz information criteria).
— Least-squares estimation procedure failed to converge due to overparameterization of model when applied to homogeneous tissue.

the three models when the usual procedure for estimating the rate constants from total tissue activity data is used are shown in Fig. 5B. Both the 4K model and the tissue heterogeneity model predict reasonably well the total tissue activity after the first 10 min. The 4K model, however, underestimates the DG and overestimates the DG-6-P concentrations throughout the experimental period but approaches the true value for DG-6-P concentration at 45 min. The same patterns of overestimation/underestimation were observed in all simulations, with the magnitude of the difference between the model predictions and the "measured" data increasing as the percentage of white matter in the mixed tissue increased.

$rCMR_{glc}$

Values of $rCMR_{glc}$ calculated by use of each of the three models for each of the mixed tissues are listed in Table 4. $rCMR_{glc}$ was calculated with <5% error when the 3K model for a homogeneous tissue was used with the rate constants fitted from the current simulation data (Fig. 6). The 4K model, which assumes loss of product, overestimated $rCMR_{glc}$ by as much as 36%. With both homogeneous tissue models (i.e., 3K and 4K models), the largest errors in $rCMR_{glc}$ occurred in those mixed tissues that were 70–80% white matter. The tissue heterogeneity model approximated the true value of $rCMR_{glc}$ to within 5%; the largest errors in $rCMR_{glc}$ occurred in tissue with 90–100% white matter. The error in $rCMR_{glc}$ calculated by use of the tissue heterogeneity model was due largely to neglecting the lag of the precursor pool behind the plasma, i.e., the second term in the denominator of Eq. 21; this term produces the largest errors in $rCMR_{glc}$ in tissues with the lowest rates of blood flow and metabolism.

DISCUSSION

The operational equation of the DG method (Sokoloff et al., 1977) is the general one used to determine the rate of a biochemical reaction in vitro with a radioactive tracer: The rate of reaction is equal to the amount of labeled product formed during a given interval of time divided by the product of the integrated specific activity of the precursor pool over the same time interval, and a correction for an

TABLE 3. *Rate constants estimated from total radioactivity in simulated heterogeneous tissue*

	Simulation no.											
	1	2	3	4	5	6	7	8	9	10	11	12
3K model												
$\hat{K}_1^*$ (ml/g/min)	0.3768	0.3407	0.3057	0.2720	0.2397	0.2092	0.1807	0.1544	0.1306	0.1097	0.0917	0.2030
SE	0.0007	0.0034	0.0058	0.0073	0.0079	0.0078	0.0071	0.0059	0.0042	0.0024	0.0005	0.0080
$\hat{k}_2^*$ (min^{-1})	0.5878	0.5443	0.4988	0.4518	0.4036	0.3550	0.3067	0.2598	0.2161	0.1777	0.1464	0.3490
SE	0.0016	0.0080	0.0141	0.0184	0.0208	0.0214	0.0201	0.0172	0.0127	0.0073	0.0015	0.0225
$\hat{k}_3^*$ (min^{-1})	0.0787	0.0755	0.0719	0.0678	0.0630	0.0575	0.0512	0.0442	0.0365	0.0285	0.0205	0.0591
SE	0.0001	0.0006	0.0012	0.0017	0.0021	0.0023	0.0024	0.0023	0.0019	0.0012	0.0003	0.0026
WRSS	9.8 $\times 10^{-6}$	3.0 $\times 10^{-4}$	1.2 $\times 10^{-3}$	2.7 $\times 10^{-3}$	4.6 $\times 10^{-3}$	6.8 $\times 10^{-3}$	8.7 $\times 10^{-3}$	9.5 $\times 10^{-3}$	8.3 $\times 10^{-3}$	4.6 $\times 10^{-3}$	3.4 $\times 10^{-4}$	7.6 $\times 10^{-3}$
4K model												
$\hat{K}_1^*$ (ml/g/min)	0.3766	0.3438	0.3116	0.2798	0.2488	0.2187	0.1898	0.1623	0.1366	0.1130	0.0923	0.2129
SE	0.0008	0.0024	0.0039	0.0050	0.0056	0.0057	0.0054	0.0046	0.0035	0.0021	0.0005	0.0060
$\hat{k}_2^*$ (min^{-1})	0.5871	0.5567	0.5232	0.4865	0.4461	0.4019	0.3541	0.3032	0.2503	0.1976	0.1499	0.3991
SE	0.0019	0.0062	0.0108	0.0147	0.0177	0.0195	0.0196	0.0180	0.0144	0.0089	0.0002	0.0213
$\hat{k}_3^*$ (min^{-1})	0.0785	0.0784	0.0779	0.0770	0.0753	0.0725	0.0682	0.0616	0.0521	0.0389	0.0226	0.0755
SE	0.0002	0.0009	0.0016	0.0025	0.0034	0.0042	0.0050	0.0053	0.0051	0.0037	0.0010	0.0048
$\hat{k}_4^*$ (min^{-1})	−0.0001	0.0011	0.0024	0.0038	0.0053	0.0070	0.0087	0.0102	0.0112	0.0102	0.0034	0.0073
SE	0.0001	0.0003	0.0006	0.0009	0.0012	0.0016	0.0021	0.0025	0.0030	0.0031	0.0014	0.0017
WRSS	9.2 $\times 10^{-6}$	1.1 $\times 10^{-4}$·	3.8 $\times 10^{-4}$*	8.2 $\times 10^{-4}$*	1.4 $\times 10^{-3}$*	2.2 $\times 10^{-3}$*	2.9 $\times 10^{-3}$*	3.4 $\times 10^{-3}$·	3.3 $\times 10^{-3}$·	2.1 $\times 10^{-3}$§	2.0 $\times 10^{-4}$§	2.5 $\times 10^{-3}$*
Tissue heterogeneity model												
$\hat{K}_1^*$ (ml/g/min)	—	0.3533	0.3256	0.2977	0.2681	0.2408	0.2119	0.1821	0.1528	0.1221	0.0945	0.2211
SE		0.0031	0.0022	0.0023	0.0029	0.0064	0.0059	0.0056	0.0039	0.0017	0.0012	0.0058
$\hat{k}_2^*$ (min^{-1})	—	0.5463	0.4939	0.4421	0.3923	0.3512	0.3061	0.2655	0.2232	0.1768	0.1489	0.3088
SE		0.0362	0.0201	0.0172	0.0179	0.0355	0.0292	0.0234	0.0151	0.0065	0.0048	0.0621
$\hat{k}_3^*$ (min^{-1})	—	0.0721	0.0650	0.0578	0.0513	0.0456	0.0398	0.0351	0.0296	0.0232	0.0199	0.0444
SE		0.0025	0.0014	0.0012	0.0012	0.0023	0.0019	0.0015	0.0010	0.0005	0.0004	0.0052
$\hat{\alpha}$ (min^{-1})	—	0.0961	0.2044	0.3275	0.4442	0.5484	0.6540	0.7537	0.7638	0.6462	0.1462	0.4841
SE		0.0499	0.0316	0.0306	0.0349	0.0785	0.0756	0.0778	0.0817	0.0631	0.0784	0.2216
$\hat{\beta}$ (min^{-1})	—	0.2443	0.2399	0.2408	0.2470	0.2454	0.2461	0.2741	0.2820	0.2700	0.2680	0.1577
SE		0.2024	0.0597	0.0377	0.0357	0.0672	0.0576	0.0581	0.0517	0.0372	0.1631	0.0845
WRSS	—	3.3 $\times 10^{-5}$*‡	2.2 $\times 10^{-5}$*‡	3.3 $\times 10^{-5}$*‡	6.8 $\times 10^{-5}$*‡	4.4 $\times 10^{-4}$*‡	5.3 $\times 10^{-4}$*‡	6.2 $\times 10^{-4}$*‡	4.9 $\times 10^{-4}$*‡	1.9 $\times 10^{-4}$*‡	1.7 $\times 10^{-4}$‡	7.4 $\times 10^{-4}$*‡

Values are estimates ± standard errors of the estimate; WRSS, weighted sum of squares of the residuals.
· Statistically significant improvement in fit over 3K model (F test, $p < 0.01$).
* Statistically significant improvement in fit over 3K model (F test, 0.005).
§ Statistically significant improvement in fit over 3K model (F test, $p < 0.05$).
‡ Improvement in fit over 4K model (by the Akaike and Schwarz information criteria).
— Least-squares estimation procedure failed to converge due to overparameterization of model when applied to homogeneous tissue.

isotope effect, if any is present. In applying this principle to the in vivo measurement of glucose metabolism with DG, the amount of product formed may be estimated from total tissue activity, and the integrated specific activity of the precursor pool may be estimated from that in plasma, provided the kinetics of the equilibration processes between the precursor pools in tissue and plasma can be described appropriately. Moreover, because of kinetic differences between DG and glucose at the hexose transport and the intracellular hexokinase sites, the conversion of the rate of DG phosphorylation to glucose utilization requires an additional factor, the so-called lumped constant, which is kinetically equivalent to an isotope effect correction factor. The original 3K model of the DG method is valid only if several key assumptions and/or conditions hold. These include the following: (a) The tissue is homogeneous with respect to rate of blood flow, rates of transport of glucose and DG between plasma and tissue, concentrations of DG, glucose, and DG-6-P, and rate of glucose utilization; and (b) DG-6-P, once formed, is essentially trapped in the tissue for the duration of the experimental procedure. When used with quantitative autoradiography to measure local tissue radioactivity and with the recommended 45-min experimental period, the 3K model of the DG method has been shown to yield

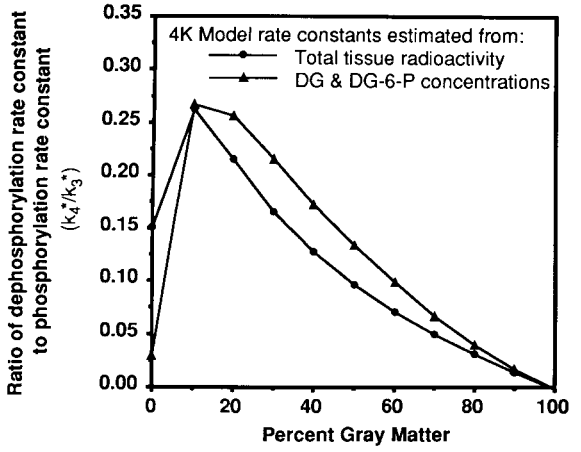

FIG. 4. Dephosphorylation rate constant for the 4K model. The nonlinear least-squares estimate of k_4^* was between 1 and 27% of the estimated value of k_3^* for the mixed tissue even though the true rate constant for dephosphorylation was actually zero. DG, deoxyglucose; DG-6-P, deoxyglucose-6-phosphate.

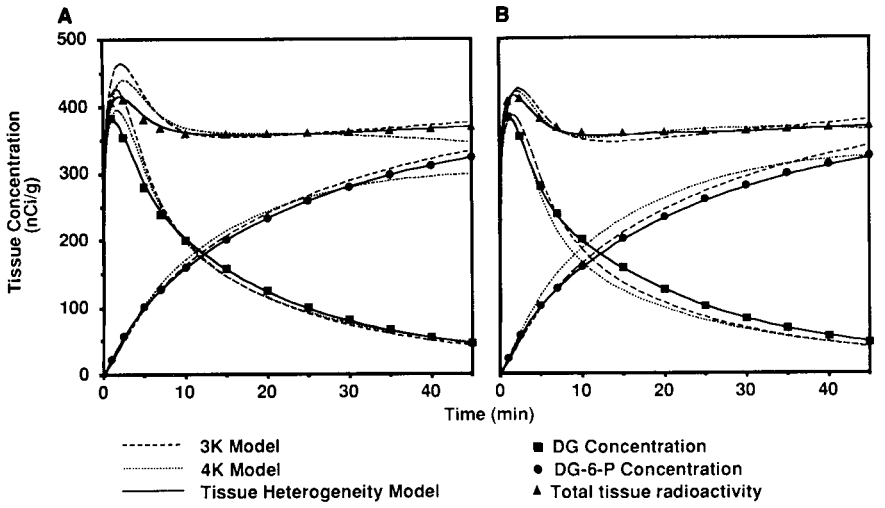

FIG. 5. Time courses of tissue concentration of deoxyglucose (DG), deoxyglucose-6-phosphate (DG-6-P), and total tissue activity predicted by each of the three models with the rate constants estimated from the DG and DG-6-P data **(A)** and the total tissue activity of the mixed tissue consisting of 50% gray and 50% white matter **(B).** If only total tissue radioactivity were known, it is clear that the effects of product loss could not be distinguished from those resulting from tissue heterogeneity, especially in the presence of noisy data. Although both the 4K and the tissue heterogeneity model predict reasonably well the total tissue activity data after the first 10 min, the 4K model consistently overestimates the DG-6-P concentration while underestimating the tissue free DG concentration.

estimates of $LCMR_{glc}$ that are time independent between 30 and 45 min after systemic tracer application and that are consistent with whole-brain metabolic rate for glucose measured by the Kety-Schmidt technique (Sokoloff et al., 1977; Sokoloff, 1985). These results indicated that, although not perfect, the model was adequate for the estimation of glucose utilization, but no physiological interpretation was given to the individual values of the parameters of the model itself. In the present study, we extended the original 3K model to include a mixture of fast and slow metabolic tissue compartments, i.e., a mixture of gray and white matter. A heterogeneous tissue is, in fact, a more realistic representation of any tissue under examination than the homogeneous tissue assumed by the 3K and 4K models. This is true with quantitative autoradiography and even more so with PET. As indicated by the results of the current simulation analysis, the average metabolic rate for glucose of a metabolically heterogeneous brain region was estimated to within ±5% at 45 min after a pulse of DG by use of either the original 3K model or the tissue heterogeneity model. This was to be expected to occur at 45

TABLE 4. *Regional CMR_{glc} ($rCMR_{glc}$; μmol/100 g/min) calculated 45 min following a pulse of deoxyglucose (DG) in simulated heterogeneous tissue*

	Simulation no.											
	1	2	3	4	5	6	7	8	9	10	11	12
True $rCMR_{glc}$	71	66	60	55	50	44	39	34	28	23	18	44
$rCMR_{glc}$ calculated using rate constants estimated from DG and DG-6-P concentrations												
3K model												
$rCMR_{glc}$	72	66	61	56	51	45	40	35	29	24	18	45
% error	1	1	1	1	2	2	2	2	3	2	1	3
4K model												
$rCMR_{glc}$	72	69	66	63	59	55	50	44	37	28	18	58
% error	1	5	9	14	19	24	28	30	29	23	2	32
Tissue heterogeneity model												
$rCMR_{glc}$	—	65	60	54	49	44	38	33	27	22	—	43
% error		−1	−1	−1	−2	−2	−2	−3	−3	−4		−2
$rCMR_{glc}$ calculated using rate constants estimated from total tissue radioactivity												
3K model												
$rCMR_{glc}$	72	67	61	56	51	46	40	35	30	24	18	46
% error	1	1	2	2	2	3	3	4	4	3	2	4
4K model												
$rCMR_{glc}$	71	69	65	62	59	55	50	45	39	30	20	55
% error	1	4	8	13	18	23	29	33	36	32	10	26
Tissue heterogeneity model												
$rCMR_{glc}$	—	65	60	54	49	43	38	33	27	22	17	43
% error		−1	−1	−2	−2	−2	−3	−3	−3	−5	−5	−2

DG-6-P, deoxyglucose-6-phosphate.
— Rate constants not available. (Least-squares estimation procedure failed to converge due to overparameterization of model when applied to homogeneous tissue.)

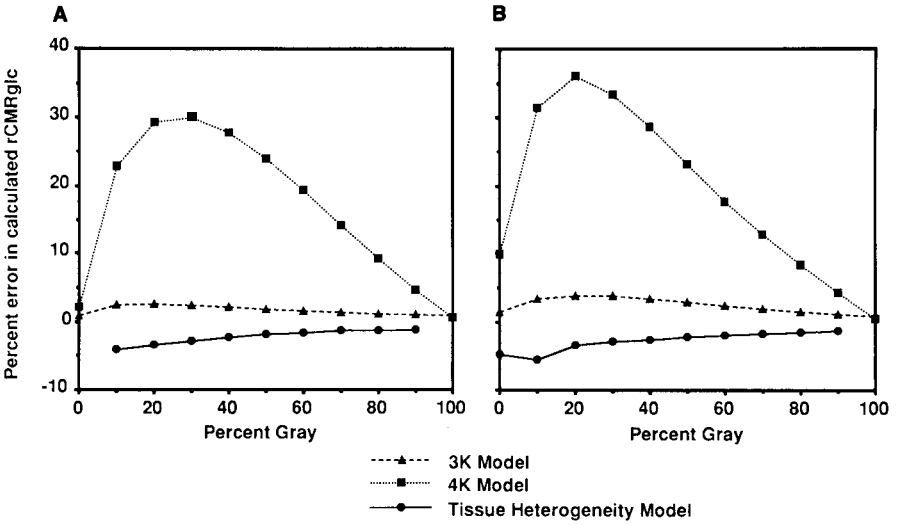

FIG. 6. Error in regional CMR_{glc} ($rCMR_{glc}$) calculated 45 min after a pulse of deoxyglucose (DG) with rate constants determined from DG and deoxyglucose-6-phosphate (DG-6-P) concentrations **(A)** and rate constants determined from total tissue activity **(B)**. Even though the loss from the simulated tissue is zero, the high estimate of k_4^*, the dephosphorylation rate constant in the 4K model, leads to the estimation of a significant amount of product loss by 45 min. Hence, the 4K model produces overestimates of $rCMR_{glc}$ up to 36%. Errors in $rCMR_{glc}$ calculated by use of the tissue heterogeneity and 3K models are not >5%.

min inasmuch as the initial differences in DG concentrations in the various compartments disappear with increasing circulation time of DG due to the equilibration between the tissue pools and the plasma. In fact, the procedure of the DG method (i.e., the use of a pulse and an experimental period of 30- to 45-min duration) was designed to minimize the influence of errors of the model rate constants and combinations thereof in determining $rCMR_{glc}$ (Sokoloff et al., 1977; Mori et al., 1990).

An important finding of the present simulation analyses is that the inclusion of both fast and slow metabolic compartments in brain tissue leads to an estimate of k_4^* significantly greater than zero even when there is no actual loss of metabolic product from the tissue in the first 45 min following a pulse of DG. High estimated values of k_4^* were found even with the most ideal data, i.e., when the tissue time courses of DG and DG-6-P concentrations were known perfectly without measurement error. Similarly, high estimates of k_4^* were also found when only the total tissue radioactivity time course was known, as would be the case in studies with autoradiography or PET. Despite the better model predictions of the time courses of tissue radioactivity that result from use of the 4K model, however, the finding of an estimated value of k_4^* greater than zero is not necessarily evidence of true loss of product. It may, rather, result from a compensation for inaccuracies in the model, namely, the assumption that the rate constant for phosphorylation, k_3^*, is constant when, in fact, the effective k_3^* in the mixed tissue actually declines with time.

The consequence of the overestimate of k_4^* found with the 4K model was a significantly overestimated $rCMR_{glc}$ in the simulated heterogeneous tissues. Thus, tissue heterogeneity provides an alternative explanation to product loss for the observed differences in $rCMR_{glc}$ calculated with different kinetic models 45 min following a pulse of FDG in PET studies. Lammertsma et al. (1987) reported that the use of the 4K model led to an estimate of k_4^* for the whole cortical rim of 0.013 min^{-1}, or 11% of the estimate of k_3^*, and to calculated values of $rCMR_{glc}$ that were 16–41% higher in whole brain than those estimated with the 3K model. In the current simulation study, the use of the 4K model led to estimated values of k_4^* on the order of 10% of the estimated values of k_3^* and a 23% overestimate of $rCMR_{glc}$ in a hypothetical mixed tissue consisting of 50% gray and 50% white matter but from which there is zero loss of product. The findings of our two studies are thus in complete agreement; our interpretation, however, is that $rCMR_{glc}$ calculated with the 4K model is an overestimation of the true rate of glucose utilization due to the tissue heterogeneity and that $rCMR_{glc}$ calculated with the 3K model is the more accurate one. Further evidence that the 4K model may overestimate glucose utilization at 45-min experimental times was provided by the value of the lumped constant for FDG in humans calculated by Lammertsma et al. (1987) from the combined measurements of oxygen and glucose utilization. When the 4K model was assumed, the calculated lumped constant was 0.75 ± 0.07 (mean ± SD). If the loss of FDG-6-P were overestimated in the calculation of $rCMR_{glc}$, it would result in a correspondingly overestimated value of the lumped constant to maintain the stoichiometric relationship of 5.6:1 for $rCMRO_2$/$rCMR_{glc}$. When the no loss (3K) model was assumed, the value reported for the lumped constant was 0.60 ± 0.05, which is in closer agreement with the measured value of 0.52 ± 0.028 (mean ± SEM) reported by Reivich et al. (1985).

The results of the current study are relevant to

the results of animal studies in which it was claimed that it is necessary to use the 4K model for the DG method, even with experimental periods of ≤45 min (Hawkins and Miller, 1987; Pelligrino et al., 1987). Hawkins and Miller (1987) found that time courses of DG and DG-6-P concentrations in freeze-blown whole brain were better described by the 4K kinetic model, which assumes loss of metabolic product, than by the original 3K DG model, which assumes no product loss; this was misinterpreted as evidence of loss of DG-6-P in the cerebral tissue early in the experimental period. Pelligrino et al. (1987) observed a declining apparent rate "constant" for phosphorylation of DG, i.e., k_3^*, in aspirated samples of cerebral cortex in the goat and interpreted this as evidence of glucose-6-phosphatase activity. In each of these studies the tissue was certainly heterogeneous, and the results are entirely consistent with those predicted by a model for a heterogeneous tissue with no loss of product, as in the current study.

While the present study shows that tissue heterogeneity alone can give the appearance of loss of product at short experimental times when no loss actually occurs, true product loss is observed at longer experimental times. Since its introduction, k_4^* has been assumed to represent a first-order rate constant for dephosphorylation of DG-6-P that was constant throughout the entire experimental period. There was no evidence to support this assumption of constancy; in fact, experimental evidence indicates that if there were such a rate "constant," it would change in magnitude with time (Sokoloff, 1982; Nelson et al., 1987). An attempt to take this change into account was made by extending the DG model for use at long experimental times to include two separate steps describing loss of DG-6-P: (a) transfer of DG-6-P from the cytosol into the cisterns of the endoplasmic reticulum and (b) hydrolysis of DG-6-P by glucose-6-phosphatase and subsequent return of the free DG to the precursor pool (Schmidt et al., 1989*a*). The present study demonstrates that the finding of a significant k_4^*, at least at early times, may not represent dephosphorylation at all. The estimate of k_4^* may become artifactually high in fitting routines to compensate for the time-changing k_3^* due to the heterogeneity of the tissue under examination. The effects of heterogeneity at early times combined with significant product loss at later times following a pulse of DG on the choice of kinetic model, on the estimates of model parameters, and on the calculated rates of glucose utilization are yet to be determined. It is clear, however, that even in the absence of measurement error, the effects of tissue heterogeneity can give the appearance of product loss and that the assumption of product loss with the 45-min experimental period recommended for the DG method can lead to an overestimation of the rates of glucose utilization.

These results point out the dilemma in choosing a kinetic model for the DG method. The original model and experimental procedure were chosen so that glucose utilization could be determined from a single static measurement of total tissue radioactivity with minimal influence from imperfections in the model and imperfect knowledge of the model rate constants. The advent of dynamic scanning capabilities with PET made it possible to measure entire time courses of tissue radioactivity in brain. This led to expanded efforts in modeling and parameter estimation, the goal of which was to fit the complete time course of tissue radioactivity. Implicit in this approach is the assumption that the model used to describe the kinetic behavior of DG in the tissue is perfect and that therefore closer dynamic fits of tissue time courses would lead to more accurate estimates of the rates of glucose utilization. Under the best of circumstances the model is not perfect. One imperfection is heterogeneity of the tissue under examination. Results from dynamic fits, however, are often used to calculate rates of glucose utilization in such a way that the influence of imperfections in the model may be magnified rather than minimized. Under these circumstances, based on the results of the current study, it would seem to be more appropriate to calculate $rCMR_{glc}$ by the static scan method at the most appropriate time to minimize effects of imperfections in the model.

APPENDIX: GLOSSARY OF SYMBOLS

α,β	rate constants (min^{-1}) describing the time-varying nature of the effective rate constants for efflux and phosphorylation in heterogeneous brain tissue
$\hat{\alpha},\hat{\beta}$	values of α and β estimated from the tissue heterogeneity model
C_e^*	deoxyglucose concentration (nCi/g) in homogeneous brain tissue
$C_{e1}^*, C_{e2}^*, \ldots, C_{en}^*$	deoxyglucose concentrations (nCi/g) in homogeneous subregions 1, 2, . . . , n of mixed brain tissue
$\overline{C}_e^*$	mass-weighted average deoxyglucose concentration (nCi/g) in heterogeneous

tissue

C^* total activity (nCi/g) in homogeneous brain tissue ($= C_e^* + C_m^*$)

$\overline{C}^*$ mass-weighted average activity (nCi/g) in heterogeneous tissue ($= \overline{C}_e^* + \overline{C}_m^*$)

C_m^* deoxyglucose-6-phosphate concentration (nCi/g) in homogeneous brain tissue

$C_{m1}^*, C_{m2}^*, \ldots, C_{mn}^*$ deoxyglucose-6-phosphate concentrations (nCi/g) in homogeneous subregions 1, 2, . . . , n of mixed brain tissue

$\overline{C}_m^*$ mass-weighted average deoxyglucose-6-phosphate concentration (nCi/g) in heterogeneous tissue

C_p^* deoxyglucose concentration (nCi/ml) in arterial plasma

C_p glucose concentration (μmol/ml) in arterial plasma

K_1^* rate constant (ml/g/min) for transport of deoxyglucose into homogeneous brain tissue

$\hat{K}_1^*$ value of K_1^* estimated from the 3K or 4K model

$K_{11}^*, K_{12}^*, \ldots, K_{1n}^*$ rate constants (ml/g/min) for transport of deoxyglucose from plasma to brain in homogeneous subregions 1, 2, . . . , n of mixed brain tissue

$\overline{K}_1^*$ rate constant (ml/g/min) for transport of deoxyglucose into mixed tissue ($=$ mass-weighted average of $K_{11}^*, K_{12}^*, \ldots, K_{1n}^*$)

$\hat{\overline{K}}_1^*$ value of $\overline{K}_1^*$ estimated from the tissue heterogeneity model

k_2^* rate constant (min^{-1}) for transport of deoxyglucose from homogeneous brain tissue to plasma

$\hat{k}_2^*$ value of k_2^* estimated from the 3K or 4K model

$k_{21}^*, k_{22}^*, \ldots, k_{2n}^*$ rate constants (min^{-1}) for transport of deoxyglucose from brain to plasma in homogeneous subregions 1, 2, . . . , n of mixed brain tissue

$k_2^*(t)$ effective rate constant at time t (min^{-1}) for transport of deoxyglucose from mixed brain tissue to plasma

$\overline{k}_2^*$ mass- and distribution space–weighted rate constant (min^{-1}) for transport of deoxyglucose from mixed brain tissue to plasma

$\hat{\overline{k}}_2^*$ value of $\overline{k}_2^*$ estimated from the tissue heterogeneity model

k_3^* rate constant (min^{-1}) for phosphorylation of deoxyglucose to deoxyglucose-6-phosphate in homogeneous brain tissue

$\hat{k}_3^*$ value of k_3^* estimated from the 3K or 4K model

$k_{31}^*, k_{32}^*, \ldots, k_{3n}^*$ rate constants (min^{-1}) for phosphorylation of deoxyglucose to deoxyglucose-6-phosphate in homogeneous subregions 1, 2, . . . , n of mixed brain tissue

$k_3^*(t)$ effective rate constant at time t (min^{-1}) for phosphorylation of deoxyglucose to deoxyglucose-6-phosphate in mixed brain tissue

$\overline{k}_3^*$ mass- and distribution space–weighted rate constant for phosphorylation of deoxyglucose to deoxyglucose-6-phosphate in mixed brain tissue

$\hat{\overline{k}}_3^*$ value of $\overline{k}_3^*$ estimated from the tissue heterogeneity model

k_4^* rate constant (min^{-1}) for dephosphorylation of deoxyglucose-6-phosphate to deoxyglucose in homogeneous brain tissue

$\hat{k}_4^*$ value of k_4^* estimated from the 4K model

$LCMR_{glc}$ local CMR_{glc} (μmol/100 g/min) in homogeneous brain tissue

$rCMR_{glc}$ regional CMR_{glc} (μmol/100 g/min) in mixed brain tissue

t time (min) after onset of ad-

ministration of deoxyglucose

$w_1, w_2, \ldots, w_n$ relative mass weights of homogeneous subregions 1, 2, . . . , n of mixed brain tissue ($\Sigma_{j=1}^{n} w_j = 1.0$)

Acknowledgment: This work was supported in part by NATO Collaborative Research Grant no. 0880/87.

REFERENCES

Hawkins RA, Miller AL (1987) Deoxyglucose-6-phosphate stability in vivo and the deoxyglucose method. *J Neurochem* 49:1941–1949

Lammertsma AA, Brooks DJ, Frackowiak RSJ, Beaney RP, Herold S, Heather JD, Palmer AJ, Jones T (1987) Measurement of glucose utilisation with [^{18}F]2-fluoro-2-deoxy-*d*-glucose: a comparison of different analytical methods. *J Cereb Blood Flow Metab* 7:161–172

Landaw E, DiStefano J (1984) Multiexponential, multicompartmental, and noncompartmental modeling. II. Data analysis and statistical considerations. *Am J Physiol* 246:R665–R677

Mori K, Schmidt K, Jay T, Palombo E, Nelson T, Lucignani G, Pettigrew K, Kennedy C, Sokoloff L (1990) Optimal duration of experimental period in measurement of local cerebral glucose utilization with the deoxyglucose method. *J Neurochem* 54:307–319

Nelson T, Dienel GA, Mori K, Cruz NF, Sokoloff L (1987) Deoxyglucose-6-phosphate stability in vivo and the deoxyglucose method: response to comments of Hawkins and Miller. *J Neurochem* 49:1949–1960

Pelligrino DA, Miletich SC, Albrecht RS (1987) Time course of radiolabeled 2-deoxy-D-glucose-6-phosphate turnover in cerebral cortex of goats. *Am J Physiol* 252:R276–R283

Phelps ME, Huang SC, Hoffman EJ, Selin CJ, Sokoloff L, Kuhl DE (1979) Tomographic measurement of local cerebral glucose metabolic rate in humans with [^{18}F]2-fluoro-2-deoxy-D-glucose: validation of method. *Ann Neurol* 6:371–388

Press WH, Flannery BP, Teukolsky SA, Vetterling WT (1986) *Numerical Recipes, the Art of Scientific Computing*. New York, Cambridge University Press, pp 521–528, 554–560

Reivich M, Alvi A, Wolf A, Fowler J, Russell J, Arnett C, MacGregor RR, Shiue CY, Atkins H, Anand A, Dann R, Greenberg JH (1985) Glucose metabolic rate kinetic model parameter determination in humans: the lumped constants and rate constants for [^{18}F]fluorodeoxyglucose and [^{11}C]deoxyglucose. *J Cereb Blood Flow Metab* 5:179–192

Sakurada O, Kennedy C, Jehle J, Brown JD, Carbin G, Sokoloff L (1978) Measurement of local cerebral blood flow with iodo[^{14}C]antipyrine. *Am J Physiol* 234:H59–H66

Schmidt K, Lucignani G, Mori K, Jay T, Palombo E, Nelson T, Pettigrew K, Holden JE, Sokoloff L (1989*a*) Refinement of the kinetic model of the 2-[^{14}C]deoxyglucose method to incorporate effects of intracellular compartmentation in brain. *J Cereb Blood Flow Metab* 9:290–303

Schmidt K, Mies G, Sokoloff L (1989*b*) Model of kinetic behavior of deoxyglucose in heterogeneous tissues in brain. *J Cereb Blood Flow Metab* 9 (suppl 1):S241

Sokoloff L (1982) The radioactive deoxyglucose method. Theory, procedure, and applications for the measurement of local glucose utilization in the central nervous system. In: *Advances in Neurochemistry, Vol 4* (Agranoff BW, Aprison MH, eds), New York, Plenum, pp 1–82

Sokoloff L (1985) Mapping local functional activity by measurement of local cerebral glucose utilization in the central nervous system of animals and man. In: *The Harvey Lectures, Series 79*, Orlando, Academic Press, pp 77–143

Sokoloff L, Reivich M, Kennedy C, Des Rosiers MH, Patlak CS, Pettigrew KD, Sakurada O, Shinohara M (1977) The [^{14}C]deoxyglucose method for the measurement of local cerebral glucose utilization: theory, procedure, and normal values in the conscious and anesthetized albino rat. *J Neurochem* 28:897–916